

JMBAvailable online at www.sciencedirect.com ScienceDirect

Three-Dimensional Architecture of Membrane-Embedded MscS in the Closed Conformation

Valeria Vásquez^{1,2}, Marcos Sotomayor³, D. Marien Cortes²,
Benoît Roux², Klaus Schulten³ and Eduardo Perozo^{2*}

¹Department of Molecular Physiology and Biological Physics, University of Virginia, Charlottesville, VA 22908, USA

²Institute of Molecular Pediatrics Science and Department of Biochemistry and Molecular Biology, Pritzker School of Medicine, University of Chicago, IL 60637, USA

³Department of Physics, University of Illinois at Urbana-Champaign, and Beckman Institute for Advanced Science and Technology, Urbana, IL 61801, USA

Received 20 September 2007;
received in revised form
24 October 2007;
accepted 31 October 2007

The mechanosensitive channel of small conductance (MscS) is part of a coordinated response to osmotic challenges in *Escherichia coli*. MscS opens as a result of membrane tension changes, thereby releasing small solutes and effectively acting as an osmotic safety valve. Both the functional state depicted by its crystal structure and its gating mechanism remain unclear. Here, we combine site-directed spin labeling, electron paramagnetic resonance spectroscopy, and molecular dynamics simulations with novel energy restraints based on experimental electron paramagnetic resonance data to investigate the native transmembrane (TM) and periplasmic molecular architecture of closed MscS in a lipid bilayer. In the closed conformation, MscS shows a more compact TM domain than in the crystal structure, characterized by a realignment of the TM segments towards the normal of the membrane. The previously unresolved NH₂-terminus forms a short helical hairpin capping the extracellular ends of TM1 and TM2 and is in close interaction with the bilayer interface. The present three-dimensional model of membrane-embedded MscS in the closed state represents a key step in determining the molecular mechanism of MscS gating.

© 2007 Elsevier Ltd. All rights reserved.

Edited by J. Bowie

Keywords: mechanotransduction; ion channels; electron paramagnetic resonance; spin-labeling; molecular dynamics

Introduction

Cells rely on tight regulation of the balance between internal and external osmotic forces to survive. In bacteria and archaea, osmoregulation is achieved by accumulation and release of solutes through active transport systems and mechanosensitive (MS) channels, respectively.^{1–3} MS channels act as indirect osmosensors in the emergency response to hypo-osmotic challenges. When water enters the cell, the turgor pressure increases and the membrane expands, reducing its lateral pressure, which leads to opening of MS channels. The subsequent release of solutes through the open MS channels alleviates turgor pressure and prevents cell lysis.⁴ The *Escherichia coli* inner membrane has several MS channels involved in this complex response.^{5,6} These channels have been

*Corresponding author. Institute of Molecular Pediatrics Science, University of Chicago, IL 60637, USA. E-mail address: eperozo@uchicago.edu.

Abbreviations used: MscS, mechanosensitive channel of small conductance; TM, transmembrane; MS, mechanosensitive; MD, molecular dynamics; EPR, electron paramagnetic resonance; WT, Wild Type; DOPC, 1,2-Dioleoyl-sn-Glycero-3-Phosphocholine; POPG, 1-Palmitoyl-2-Oleoyl-sn-Glycero-3-[Phospho-rac-(1-glycerol)] (Sodium Salt); DOGS-NTA, 1,2-Dioleoyl-sn-Glycero-3-[N(5-Amino-1-Carboxypentyl)iminodiAcetic Acid]Succinyl] (Nickel Salt).

classified, according to their single-channel conductance and the tension required to activate them, as MS channel of large, small, and mini conductance, or MscL, MscS/MscK, and MscM, respectively.⁴

MscL and MscS X-ray crystal structures^{7,8} have provided an important framework for understanding the gating of MS channels and interpreting experimental results. However, while both MscL and MscS seem to respond to similar bilayer deformations and the MscL structure has led to explicit modeling of its open and closed conformations,^{9–14} the MscS gating mechanism and the functional state depicted by its crystal structure remain unclear. The MscS crystal is a homoheptamer with three trans-

membrane (TM) segments per subunit (TM1, TM2, and TM3A-B) and a large cytoplasmic domain featuring seven side “windows” and a narrow opening at the region most distal from the membrane (Fig. 1a and b). The first 26 residues of the NH₂-terminus, a region that appears to play a role in gating and stability, are not resolved in the crystal structure. As the narrowest point along the permeation path is ~7 Å in diameter, it was originally suggested that this conformation represented the open state of MscS,⁸ its dimensions putatively supporting its 1-nS single-channel conductance and slight selectivity towards anions. Molecular dynamics (MD) and continuum simulations have systematically shown that

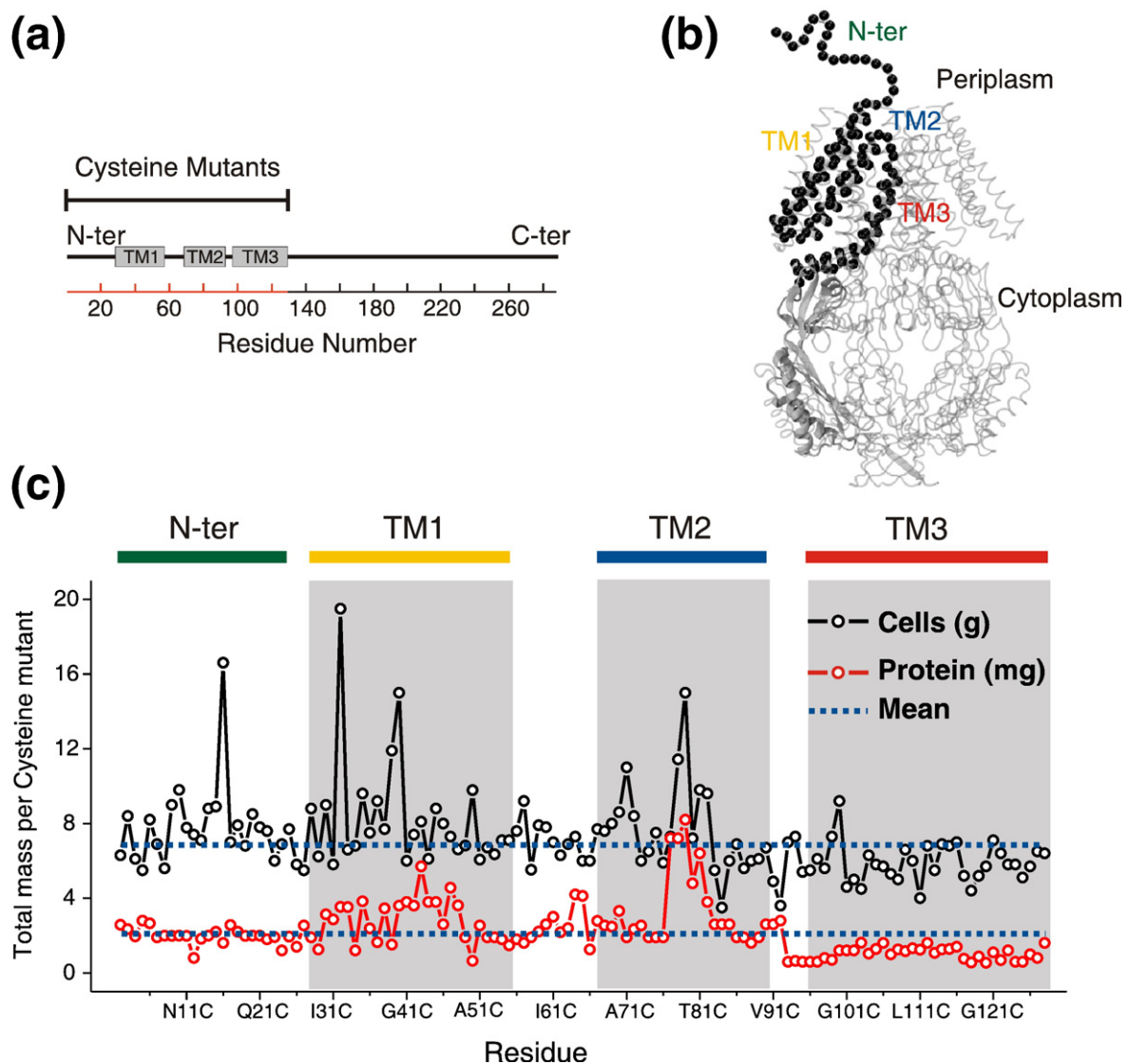


Fig. 1. MscS architecture and cysteine mutant expression. (a) Linear representation of MscS topology. The TM helices (as suggested from the crystal structure) of the MscS monomer (TM1, TM2, and TM3) are represented by rectangles. The scale corresponds to the amino acid residue numbering. The red line denotes the residues that were mutated to cysteine. (b) Single MscS subunit showing amino acid residues (black spheres) probed through site-directed spin labeling of cysteines. A single MscS monomer is represented as part of the heptamer according to the crystal structure of the channel. The NH₂-terminal segment (26 residues) is represented by a schematic line. (c) Expression of cysteine mutants. The total amount of cell and protein obtained is shown for each residue after expressing single cysteine mutants in vector pET28 (containing MscS with His₆ epitope at the NH₂-termini) in *E. coli* RosettaTM cells. Gray areas represent the membrane-embedded areas derived from the MscS crystal structure.

the crystal conformation exhibits low conductance, rectification at high voltages, and high anionic selectivity.^{15–20} Hence, while the current consensus is that the MscS crystal conformation is unlikely to represent the fully open state, its precise functional assignment remains to be established. It is then clear that to determine the conformations of the closed and open states and thereby understand the mechanogating process underlying MscS function *in vivo*, additional structural and dynamical information on MscS in a native-like membrane is required.

Electron paramagnetic resonance (EPR) spectroscopy is a powerful tool for structural analysis of soluble and membrane proteins in native-like conditions. This technique is particularly useful for judging crystal structures obtained in non-native environments.^{9,21–23} Site-directed spin labeling and EPR spectroscopy give three types of structural information: spin-label motion, solvent accessibility, and distance measurements.^{21,24} It is therefore possible to determine whether a spin-labeled position is exposed to the solvent or the membrane, or buried within the protein. Altogether, the EPR data in the context of a lipid bilayer, along with computational methods, offer an extensive collection of accessibility constraints that considerably decrease the number of possible folds in order to derive three-dimensional models of proteins in their native environments and in different conformational states.^{25–27}

Here we have analyzed the structural dynamic properties of membrane-reconstituted MscS in the closed-state conformation, as determined by site-directed spin labeling, EPR spectroscopy, and computational modeling. The experimental data were used to refine the crystal structure under known physiological conditions and to construct a model of the closed conformation of MscS that includes the previously unresolved NH₂-terminus. The new model shows significant differences regarding the position of the TM1–TM2 hairpin and the arrangement of TM2 with respect to TM3. We find that the NH₂-terminus is a mixed helical hairpin, placed at the periplasmic interface of the lipid bilayer, away from the channel central axis of symmetry. Our experimental data suggest that the MscS closed state is in a different and more compact conformation than the one trapped in the crystal structure.

Results

Expression and purification of MscS cysteine mutants

Individual residues along the complete TM domain of MscS were sequentially mutated to cysteine and subsequently spin labeled (wild-type (WT) MscS is cysteineless). The targeted regions are highlighted in Fig. 1a along a schematic representation of the MscS sequence, where individual rectangles represent the approximate length of the α -helical TM segments according to the crystal structure.⁸ The mutated residues (2–128) are shown in Fig. 1b as black spheres on a ribbon diagram of the MscS

monomer and over a schematic line in the structurally undetermined NH₂-terminus.

All MscS cysteine mutants were expressed, purified under reducing conditions, labeled, and reconstituted into pre-formed 1,2-Dioleoyl-sn-Glycero-3-Phosphocholine (DOPC):1-Palmitoyl-2-Oleoyl-sn-Glycero-3-[Phospho-rac-(1-glycerol)] (Sodium Salt) (POPG) liposomes as previously described.²⁸ None of the mutations were associated with significant gain of function phenotypes that would result in lethal leakage of solutes during cell growth, since the culture's optical density did not decrease upon induction with IPTG. Instead, some cysteine substitutions at conserved sites⁸ promoted cell growth (W16C at the NH₂-terminus, V32C and V40C at TM1, and A79C at TM2).

Mutant expression yield was in general below that of WT MscS (~4 mg, Fig. 1c), and even lower for mutations at the NH₂-terminus and the TM3 helix. Despite these differences, heptameric oligomerization was always achieved. This suggests that mutant purification under reducing conditions did not affect the overall architecture of the channel; that is, the heptameric structure is not compromised in the formation of spontaneous disulfide bridges, as suggested by gel filtration analysis and SDS-PAGE gels (Supplementary Fig. S1). Mutations on the narrowest part of the MscS permeation pathway (positions 93–101, 107, and 115) promoted some dissociation of the heptamer into an unfolded channel, which represented a small fraction of the total protein.²⁸ For these particular TM3 mutants, EPR spectroscopy was performed on the fraction that corresponded to the heptamer, as determined by gel filtration analysis (Supplementary Fig. S1).

Environmental parameters of MscS TM segments

Spin-labeled mutants were subjected to continuous wave EPR spectroscopic measurements on liposomes, under zero transbilayer pressure and in the absence of a TM voltage. It is expected that under these conditions, the spectroscopic signal will come overwhelmingly from MscS in its closed state (Supplementary Fig. S2), with negligible contributions from other conformations. Nitroxide mobility and accessibility to O₂ and NiEdda were measured for each MscS spin-labeled mutant, and accessibility to the lipid Ni(II) chelate (1,2-Dioleoyl-sn-Glycero-3-[[N(5-Amino-1-Carboxypentyl)iminodiAcetic Acid] Succinyl] (Nickel Salt) (DOGS-NTA)) was evaluated in selected mutants at the NH₂-terminus, TM1–TM2 loop, and at the end of the TM3B. It must be noted, however, that we have been unable to estimate intersubunit distances or proximities in the present data set. This is likely due to underlabeling of samples caused by the presence of genomic MscS monomers (Supplementary Fig. S3). The high natural abundance of these cysteine-less monomers in the population of heptameric channels sharply reduces the probability of finding spin-spin coupling between adjacent subunits and limits our ability to determine

intersubunit distances. However, this fact does not affect the quality and usefulness of the environmental data from under-labeled channels.

A representative set of EPR spectra obtained for MscS TM1 is shown in Fig. 2a. The fully processed EPR environmental data set for the NH₂-terminus and TM segments is shown in Fig. 2b. Mobility and O₂ accessibility parameters indicate a clear trend for the dynamics and membrane exposure of the TM domain. When the first 26 residues of the NH₂-terminus (see analysis below) are excluded, residues located towards the NH₂-terminal region of TM segments, periplasmic face of TM1, and cytoplasmic face of TM2, are more mobile and more exposed to O₂ than those at the COOH-terminal. Average mobility and O₂ accessibility (top and middle panels in Fig. 2b, respectively) were higher in TM1 and at the NH₂-terminal segment of TM2 than those obtained for TM3. On the other hand, the EPR data suggest that the environment of TM3 helices is sterically restricted, as reflected by a lower O₂ exposure and lower overall dynamics than seen for the remaining TM helices (see box plots in Fig. 5b). This behavior is expected for a segment that lines the conduction pathway of an ion channel in its closed conformation. A patch of the TM3 segment (positions 104 to 112) exhibits higher mobility and O₂ accessibility than the TM3 average (dotted box on middle panel of Fig. 2b). This can be interpreted to support the hypothesis that the ion flow may be blocked by the hydrophobicity of the surface that contours the pore in the closed state.¹⁶

Although the MscS crystal structure was obtained in detergent, the EPR-derived environmental data mapped onto its surface (Figs. 2c and 8a) reveals interesting correlations between the two types of structural data. However, probe dynamics and exposure to aqueous environment in the TM1–TM2 connecting loop (upper and bottom panels in Fig. 2b and c) appear to be inconsistent with the boundary between TM1 and TM2 segments predicted by the crystal structure.⁸ Positions exposed to NiEdda at the TM1–TM2 hairpin appear to be in the nonpolar region of the membrane (bottom panel in Fig. 2c), while highly mobile and O₂-exposed residues tend to locate at the cytoplasmic region of TM2 (upper and middle panels in Fig. 2c and left panel in Fig. 8a). As NiEdda-accessible residues seem to cluster toward the COOH-terminal end of TM1 (bottom of Fig. 2c and middle panel in Fig. 8a), we would suggest that to match the membrane

boundaries to the experimental data, these should shift about two turns of the helix towards the extracellular face of the channel in relation to putative boundaries based on the crystal structure.

Residue solvent accessibility values obtained using hard-sphere methods on the crystal structure were used to calculate TM1 and TM2 environmental moments, which were compared with the O₂ accessibility (ΠO_2) resultant moment obtained from EPR data (Supplementary Fig. S4). The position of the resultant vectors agrees with the TM1 being exposed to two environments (lipidic and proteinaceous), and the TM2 COOH-terminal region facing a proteinaceous homogenous environment. For TM3, environmental moments could not be calculated, since overall mobility and accessibility were low compared to those of the other TM segments. Within this segment, however, residues G104C-SL to Q112C-SL exhibited higher O₂ accessibility than the TM3 average. Although the overall topology suggested by EPR environmental parameters in a membrane environment is consistent with that depicted by the available MscS crystal structure, the data suggest that the closed conformation of MscS has to feature a TM2 helix that is packed against TM3. This suggests a more compact arrangement of the TM helices relative to each other and shifted downwards in relation to the plane of the bilayer.

To assist us in predicting the position of the MscS TM domain with respect to the membrane, we used DOGS-NTA[Ni(II)]lipids as a probe of residue interfacial positioning. These synthetic lipids confine the Ni(II) relaxing agent within a region of 14 Å at the membrane–aqueous interface (14 Å being the maximum distance in the lipid extended configuration; Fig. 3a).²⁹ Figure 3b and c show the DOGS-NTA collisional frequency data obtained for positions at the end of TM1 and the beginning of TM2. We used two contrasting residues in the middle of the bilayer as experimental controls in order to set the background collisional levels; I39C-SL is one of the positions most exposed to O₂ in the core of the membrane, while G41C-SL is one of the most buried ones (see red arrows in Fig. 3b). According to these environmental parameters, the TM1–TM2 loop (positions 50–61) and positions M126C-SL, F127C-SL, and R128C-SL are at the membrane–aqueous interface, and positions N53C-SL, R54C-SL, K60C-SL, and A63C-SL are largely exposed to the aqueous compound NiEdda.

Fig. 2. EPR spectroscopy of MscS. (a) Representative X-band EPR spectra of consecutively spin-labeled mutants from TM1 segment of MscS reconstituted in DOPC:POPG liposomes. All spectra were obtained from samples with the same protein-to-lipid ratio, and using a loop-gap resonator with the microwave power set to 2 mW. (b) Residue-specific environmental parameter profiles obtained for the NH₂-terminal and TM segments: mobility parameter ΔH_0^{-1} (top, black circles), O₂ accessibility parameter ΠO_2 (middle, red squares; the dotted box pinpoints the patch of higher O₂ accessibility in TM3), and NiEdda accessibility parameter $\Pi NiEdda$ (bottom, blue triangles; the broken line represents the NiEdda average for the TMs). Gray areas represent the TM segment assignment derived from the MscS crystal structure. (c) Residue environmental parameter profiles mapped onto a molecular surface of two representative MscS monomers. Mobility parameter ΔH_0^{-1} (top panel), O₂ accessibility parameter ΠO_2 (middle panel), and NiEdda accessibility parameter $\Pi NiEdda$ (bottom panel). Arrows on bottom panel pinpoint residues with high NiEdda accessibility in the middle of the bilayer.

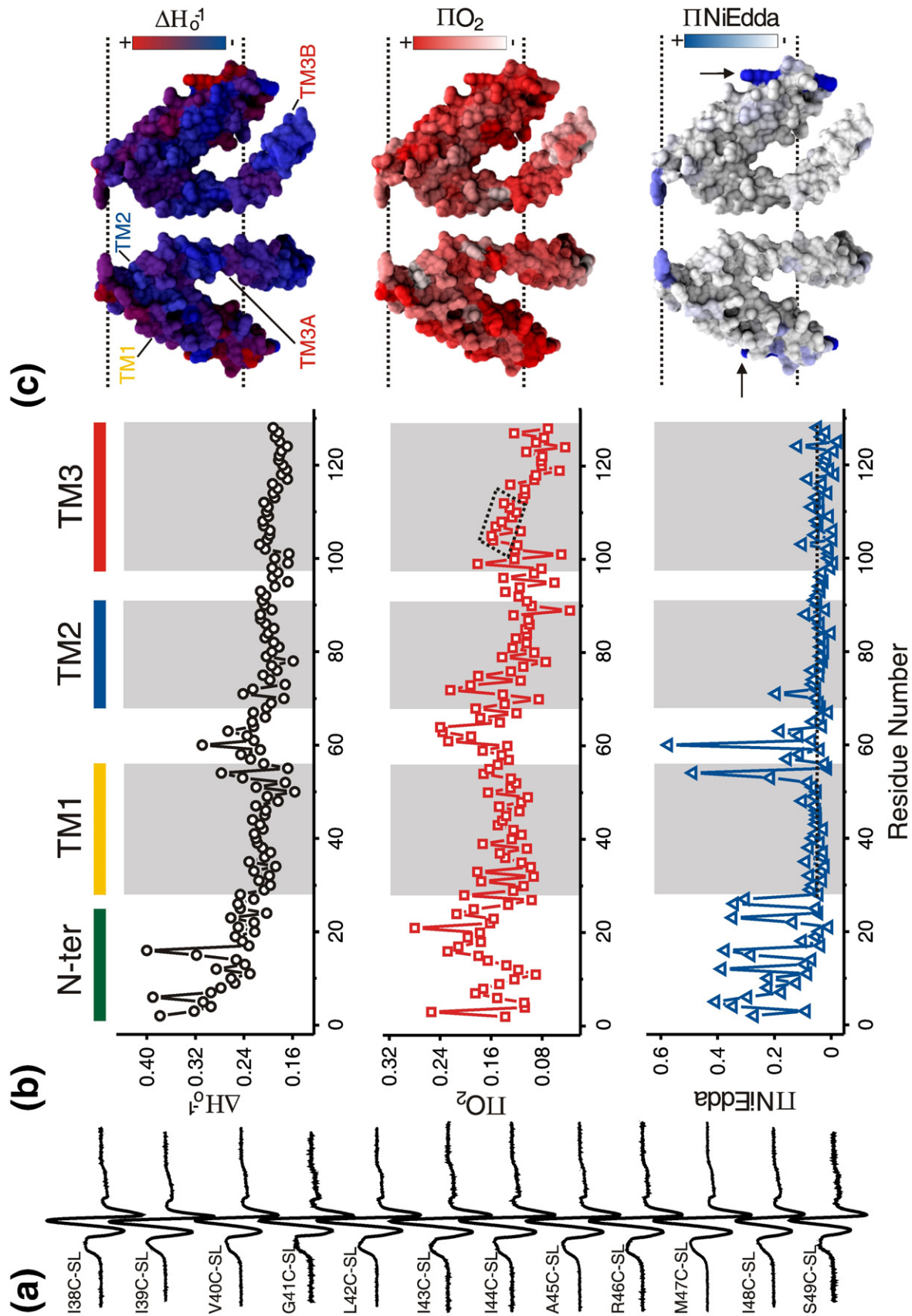


Fig. 2 (legend on previous page)

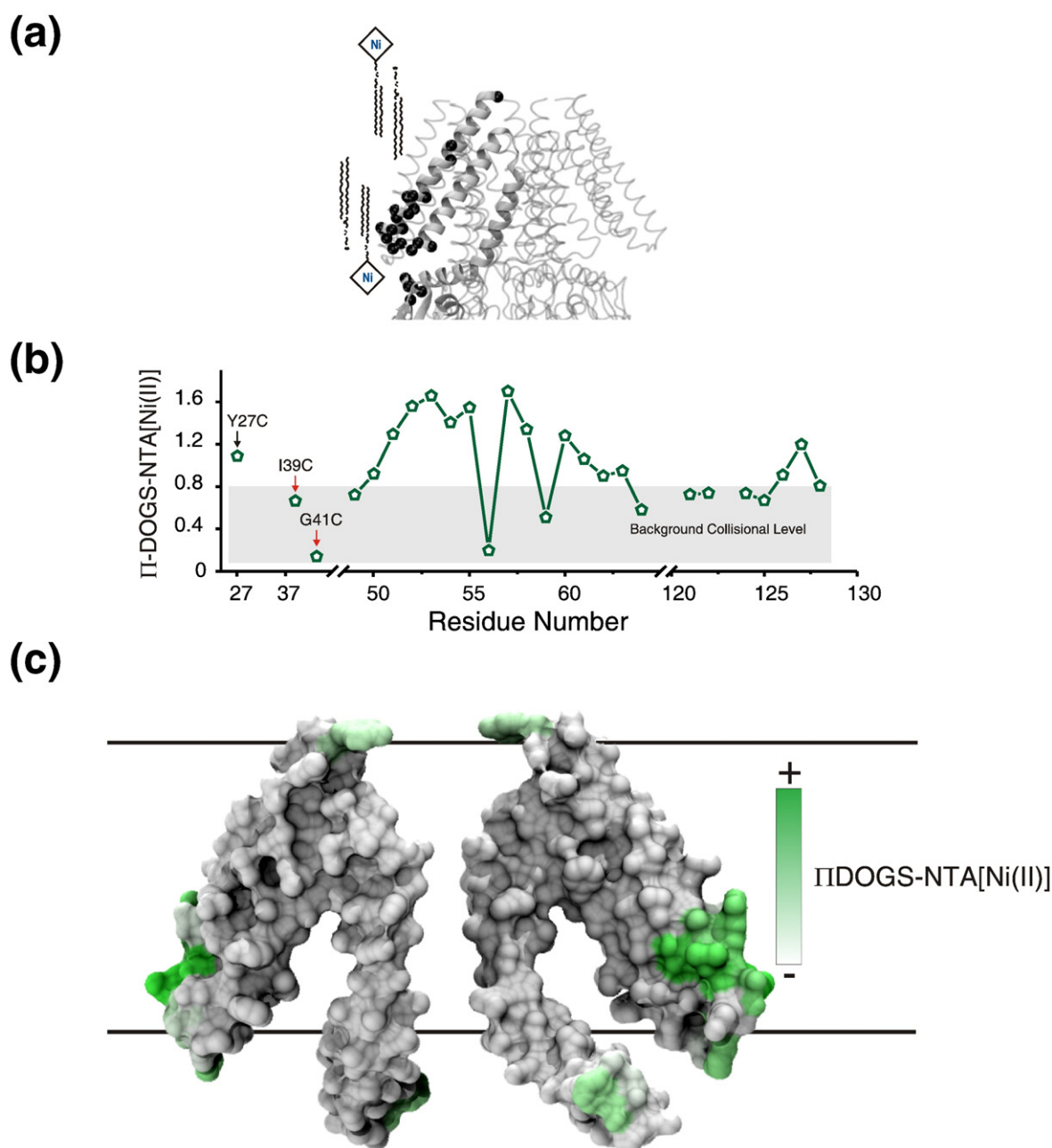


Fig. 3. Identification of MscS interfacial residues with DOGS-NTA[Ni(II)]lipids. (a) Ribbon diagram of the TM segments of the MscS crystal structure (a single MscS monomer is highlighted) embedded in a schematic membrane consisting of DOPC:POPG and DOGS-NTA[Ni(II)]lipids (few lipid molecules are shown for clarity). Black spheres show the location of cysteine mutants that were used to obtain the data. (b) Residue environmental parameter profile derived from Y27C (black arrow), TM1-TM2 loop, and TM3B. Experimental controls (I39C and G41C) are identified with red arrows. The gray box highlights the region that corresponds to background collisional level. (c) Results mapped onto a molecular surface of MscS TM segments in their crystal conformation.

Conformation of the NH₂-terminal segment

The majority of the studies performed on MscS so far have focused on its TM segments^{30–33} or its large cytoplasmic domain,^{34,35} but not on the structurally unknown NH₂-terminus. The MscS NH₂-terminal segment, comprising 26 residues, was not resolved in the MscS crystal structure.⁸ However, functional experiments show that NH₂-terminal truncation

affects protein expression but not the ability of the channel to protect the cell during hypo-osmotic challenges.³⁰ To establish any functional effect of the mutated cysteines on the channel function, after protein over-expression, cells were subjected to a sudden osmotic downshock and cell survival assay (Fig. 4a).²⁸ The majority of the cysteine mutants (73%) had no effect on the response of MscS to hypo-osmotic shock, 19% had a partially impaired response (V7C,

N11C, A13C, V18C, and L25C), and only 8% experienced severe loss-of-function mutants (V6C and A19C), that is, channels that did not open upon increase in membrane tension by the osmotic downshock. Regardless of their particular functional phenotype, all of the NH₂-terminal mutants were found to be heptamers after purification. These loss-of-function phenotypes (likely caused by channels locked in a closed state) were not disregarded in the present analysis, since this study only covers the closed conformation of MscS.

To accurately evaluate the structure of the NH₂-terminal region, we used an expression vector with the His-tag on the COOH-termini.²⁸ Under these conditions, the NH₂-terminus appears as a highly mobile fragment (Figs. 4b and 5b) with well-defined segments of secondary structure. The spectral line shape and mobility values are of the motional regime found on residues at the surface of soluble proteins.²¹ The NH₂-terminus mobility profile (Fig. 4c, top panel, black trace) shows a slight decrease in probe dynamics, from residue E2C-SL to the point of initiation of TM1, with the exception of positions V6C-SL and W16C-SL, which have high mobility values, an indication of local unfolding (loop or hinge region). O₂ accessibility, shown in Fig. 4c, mainly reveals a valley (S9C-SL up to A13C-SL) and a peak (W16C-SL up to L25C-SL) of accessibilities, whereas NiEdda clearly reveals an α -helical pattern. Calculation of the Fourier transform power spectrum of the NiEdda accessibility profile gives a statistically significant peak of angular frequency of 100° (Supplementary Fig. S6), confirming the presence of an α -helical structure. Figure 4c (bottom panel) shows the DOGS-NTA collisional frequency, suggesting that the NH₂-terminus is located at the membrane interface. One segment of the NH₂-terminus is exposed to the hydrated side of the membrane (positions 4–6, 12, 22–23, and 26–27), while another one is exposed to the membrane fatty acid chains (positions 3, 7–9, 17–22). S15C-SL and W16C-SL have high accessibilities to both contrasting agents, but W16C-SL does not have much accessibility to the Ni(II) lipid chelate; this could account for the S15C-SL facing the membrane interface and the W16C-SL pointing towards the pore.

We have used this set of environmental data to assign the secondary-structure elements within the NH₂-terminus. Figure 5a shows individual environmental moments for the residues in this mutant set and the vectors superimposed on a helical wheel plot. The resultant O₂ moment points to the face with the highest accessibility (positions G14C-SL, L17C-SL, and Q21C-SL), therefore, to the hydrophobic part of the membrane, while the NiEdda moment is oriented about 180° away, mostly defined by positions G12C-SL, L23C-SL, and S26C-SL. Overall, these results establish the NH₂-terminus as an amphipathic helix lying at the membrane interface. A comparison between the NH₂-terminus and the three TM segments (Fig. 5b) leads us to suggest that this amphipathic segment, as a whole, is likely

extending away from the channel pore, since its average mobility and accessibility are higher than those of the TM domain. Application of the sliding α -periodicity index window helped us define statistically significant α -helical regions within the NH₂-terminal segment^{36,37} (Fig. 5c). This information was used to carry out an unbiased assignment of two α -helical segments, from I10 to G14 and N20 to Y27. These assignments served as the starting point for further refinement of our final three-dimensional MscS model.

Three-dimensional model for the NH₂-terminus and TM segments of MscS in the closed state

The present data set provides information-rich constraints (128 constraints, each with 3 degrees of freedom) to refine the molecular architecture of closed MscS in its membrane environment. Using the available crystal structure of MscS as a starting point, we generated a structural model of the NH₂-terminus of MscS in the closed state driven by the EPR environmental data. The starting model was based on a sevenfold symmetric structure that included an NH₂-terminal conformation predicted by the program Rosetta,^{38,39} as well as the MscS crystal (PDB code 2OAU⁴⁰) covering residues 27 to 178 (Fig. 6a). Constraints on the secondary structure of the NH₂-terminus (α -helix between residues 10 and 14, and 20 to 27) were incorporated based on frequency analysis of the angular periodicity components of the NiEdda accessibility profile (see Fig. 5c). Structural refinement was carried out using a newly developed approach that takes advantage of EPR-determined solvent accessibility restraints in MD simulations⁴¹ (Sompornpisut *et al.*, unpublished data). In this approach, pseudoatoms representing EPR spin-label probes are attached to each MscS residue (from positions 1 to 178; Fig. 6b) and interact with pseudoatoms that represent NiEdda and O₂ molecules (Fig. 6b, inset). Their interactions were chosen to enforce the environments detected in the EPR experiments (aqueous, lipidic, buried in protein, membrane interface, or undetermined) as summarized in a phase diagram shown in Supplementary Fig. S7.

MD simulations including the EPR constraints and probes mentioned above, together with local adjustments to ensure orientation of residues at the membrane interface, permitted a dynamic refinement of MscS. The resulting MscS model, shown in Figs. 6b (NH₂-terminus) and 7, satisfies the mobility and accessibility data by compacting the TM1–TM2 helices against the pore, featuring a reorientation of these two helices (of ~9°) with respect to the normal of the membrane, and narrowing the pore lined by the TM3 helices. Interestingly, within the channel context, the NH₂-terminal conformation exhibits an amphipathic segment with α -helical regions at the membrane interface, which must face away from the center of the channel in order to fit the mobility and accessibility data. As expected, the experimental data mapped onto the surfaces of the resulting

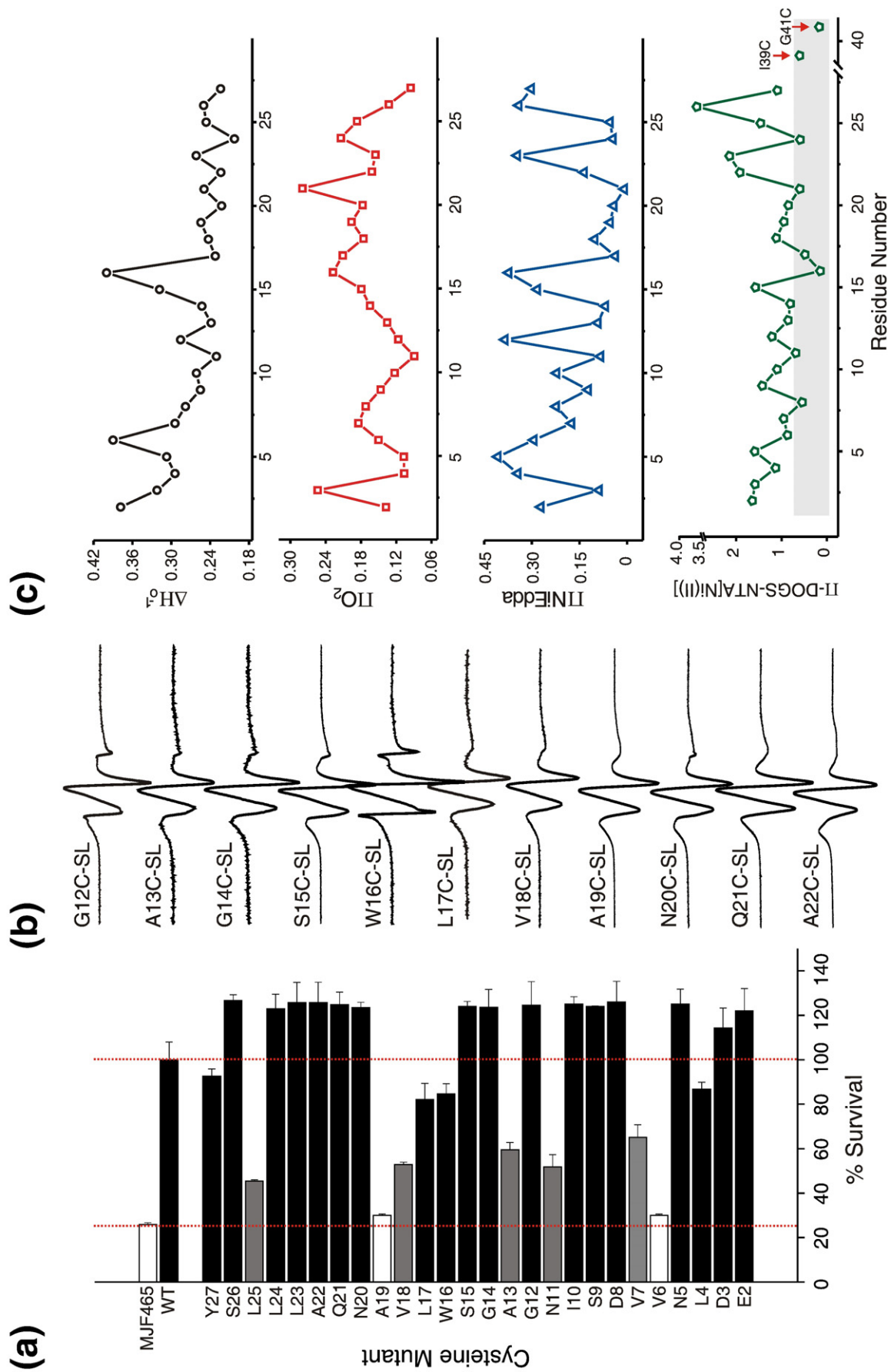


Fig. 4 (legend on next page)

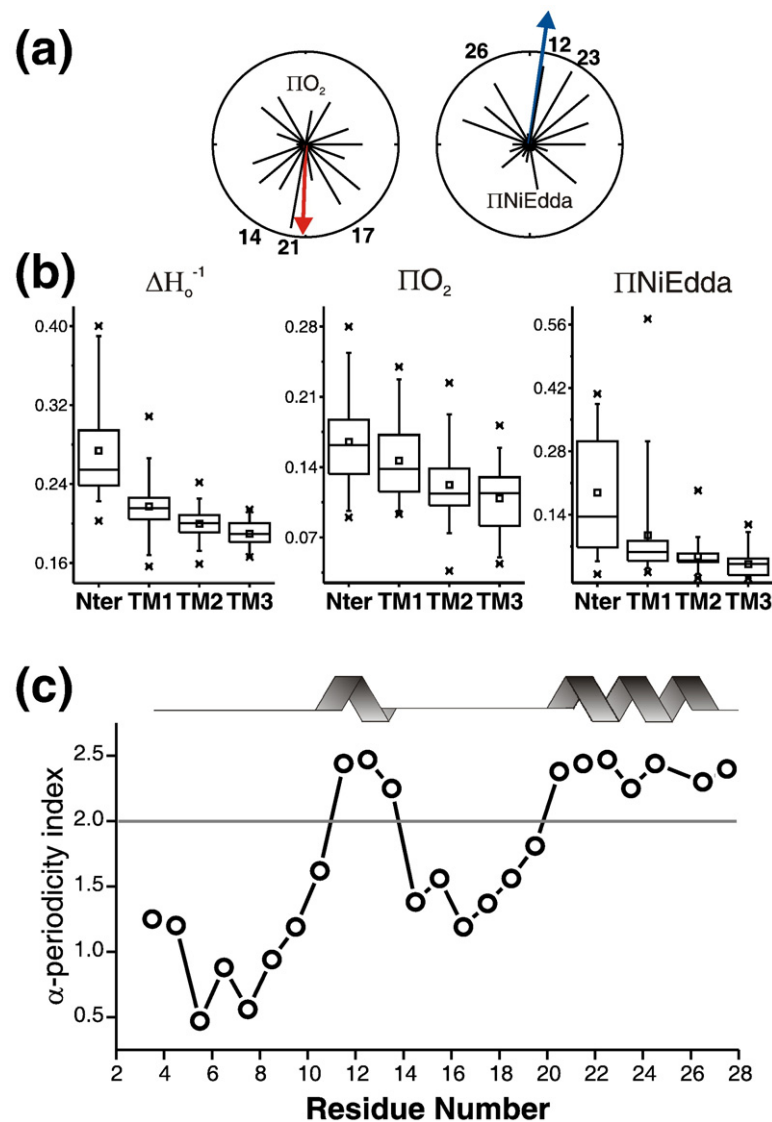


Fig. 5. Structural analysis of the NH₂-terminal segment. (a) Helical wheel representation of the NH₂-termini. Environmental parameters have been superimposed in a polar coordinate representation. A resultant vector was calculated for the O₂ accessibility (left panel, red arrow) and NiEdda accessibility (right panel, blue arrow). (b) Box plot analysis of the NH₂-termini and TM segments environmental parameters. Squares represent the mean, boxes the data distribution, and bars the standard deviation. (c) Windowed periodicity analysis for the NiEdda parameter $\Pi NiEdda$. The α -helical periodicity index was calculated as described earlier³⁶ with an angular range of 80°–120° and a sliding window of seven residues. The horizontal line represents the threshold at which the periodicity of the windowed segment is significantly α -helical (10 to 14 and 20 to 27).

model of the MscS closed state are consistent with the obtained conformation (Fig. 7a–e).

The stability of the resulting symmetric model was then probed through all-atom MD simulations of MscS in an explicit, fully hydrated membrane environment (Supplementary Fig. S8A). The structure remained reasonably stable during 6 ns of free dynamics (without any symmetric constraint; Supplementary Fig. S8B). The RMSDs of the complete model and of the TM domain alone reached values of 3.5 and 2.6 Å, respectively (Supplementary Fig. S8E). The larger value observed for the complete structure likely reflects the high mobility of the NH₂-

terminus. In fact, four of seven subunits keep their initial architecture, but partially lose their initial secondary structure.

The RMSD values observed for the EPR-based model were found to be similar to those observed for the MscS crystal structure (PDB code 2OAU), which closes asymmetrically when simulated in a relaxed membrane environment (see Supplementary Fig. S8C and D). Two additional simulations of the EPR-based closed model were performed at ± 1.2 V (3 ns each). The simulations demonstrated that the structure indeed represents a conformation of very low conductance (data not shown). Water penetration

Fig. 4. Functional and residue-specific environmental parameter profiles of NH₂-terminal cysteine mutants. (a) Functional assays of cells containing NH₂-terminal cysteine mutants overexpressed in pQE70 vector. MJF465 and WT MscS were used as negative and positive controls, respectively. Red dotted lines represent the mean values of WT MscS (right) and MJF465 (left). (b) Representative X-band EPR spectra of consecutively spin-labeled mutants from the NH₂-terminal segment of MscS reconstituted in DOPC:POPG liposomes. (c) Residue-specific environmental parameter profiles obtained for the NH₂-terminal segment: mobility parameter ΔH_o^{-1} (top, black circles), O₂ accessibility parameter ΠO_2 (middle, red squares), NiEdda accessibility parameter $\Pi NiEdda$ (middle, blue triangles), and interfacial accessibility parameter $\Pi DOGS$ -NTA[Ni(II)]lipids (bottom, green rhombuses). The gray box highlights the region that corresponds to background collisional level.

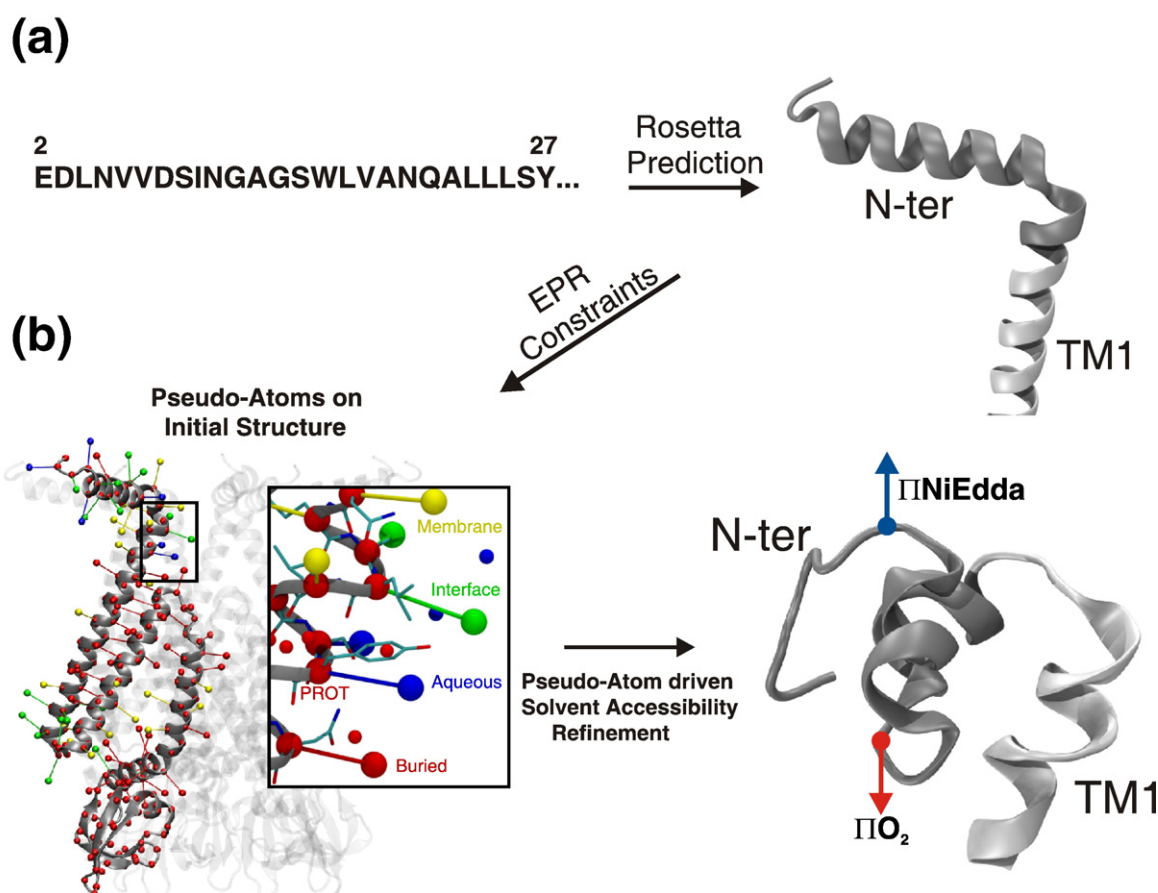


Fig. 6. Topology and structural model of MscS NH $_2$ -terminal domain obtained by the pseudoatom-driven solvent-accessibility refinement. (a) Secondary structure prediction, from the linear sequence (left panel) of residues 1 to 178, using the software Rosetta.^{38,39} The right panel shows a conformation of the NH $_2$ -terminal domain obtained after energy minimization of the predicted model. The resulting structure was used in the EPR-based refinement of the MscS closed conformation. (b) Left panel, cartoon representation of MscS model used as initial structure for refinement. The model includes residues 1 to 178. Pseudoatoms representing the spin label attached to each residue are shown for one subunit and color coded as follows: red particles represent buried residues, blue particles represent aqueous residues, yellow particles represent residues facing the membrane, and green particles represent residues at the water-membrane interface. Red particles are shown for each C α atom representing PROT particles attached to each residue. Inset shows protein residues in thin licorice representation and pseudospin probes in CPK representation. Unbounded particles in red and blue represent O $_2$ and NiEdda virtual environment particles, respectively. View of the NH $_2$ -terminal model after pseudoatom-driven solvent accessibility refinement is shown on the right panel. Residues 1 to 28 are shown in gray; resultant vectors for NiEdda and O $_2$ accessibilities are shown in blue and red, respectively.

into the periplasmic mouth of the channel observed throughout simulations, along with the NiEdda accessibility data, suggests that the periplasmic channel region might be even more occluded than what the EPR-based model predicts. Finally, it is interesting to note that the model predicts formation of a salt bridge between residues 62 and 128 of adjacent subunits, likely relevant for MscS function.¹⁵

Discussion

Membrane proteins are a fundamental part of the cell machinery, serving as switches, sensors, and bridges between the extracellular and intracellular space. However, establishing the correlation between structure and mechanism is fraught with difficulty. X-ray crystallography can provide a detailed

atomistic view of a membrane protein, but crystallization in the absence of a native-like lipid environment has the potential to induce a non-physiological conformation.⁴¹ Particularly, for the MscS channel it is very important to know its conformation in the membrane, since its gating relies on the direct interaction with the lipid bilayer.³³ Determining what functional state is depicted by the crystal conformation is extremely challenging, particularly when large conformational changes arise from external stimuli. MS channels undergo such large rearrangements in their structure upon application of mechanical stimuli, as has been shown in MscL.¹¹ Unambiguous identification of MscS closed, open, and inactive conformations is an essential step in the quest to understanding its gating mechanism and function in bacterial cells and mechanosensation in general.

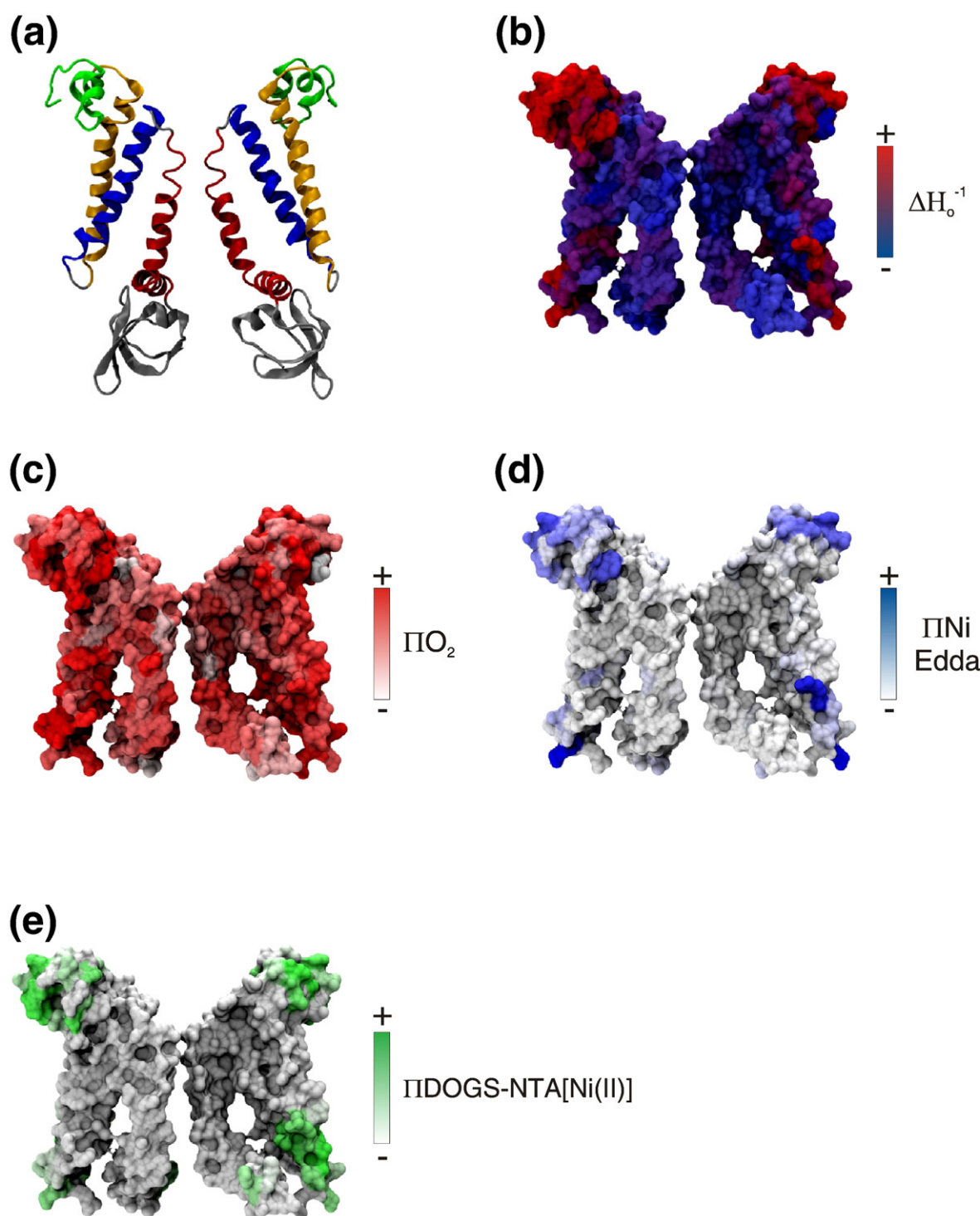


Fig. 7. MscS closed conformation obtained from EPR-based refinement. (a) Ribbon representation of the MscS closed-state model (two subunits are shown for clarity). Individual TM segments are color coded as follows: NH₂-terminus, green; TM1, yellow; TM2, blue; and TM3, red. (b) Mobility parameter ΔH_o^{-1} , (c) O₂ accessibility parameter ΠO_2 , (d) NiEdda accessibility parameter $\Pi NiEdda$, and (e) interfacial accessibility parameter $\Pi DOGS-NTA[Ni(II)]$ lipids.

The present study focuses on determining the three-dimensional fold of the MscS NH₂-terminus and TM domain when MscS is in its closed conformation, embedded in a lipid bilayer. EPR spectroscopy analysis of spin-labeled mutants provided information on the topology and secondary and tertiary structure of MscS under native condi-

tions. This information was used, along with MD simulations, to evaluate a recently further refined crystal structure⁴⁰ and propose a model of MscS in a closed conformation.

The EPR data show that there are general similarities between the overall structure and topology of MscS in a biological membrane and in the crystal

conformation. However, some differences point to the fact that the MscS crystal structure does not represent the true closed state, unlike MscL where differences between the crystal structure and the structure suggested by the EPR data are more subtle.⁹ The accessibilities to the water-soluble compound NiEdda indicate that positions at the cytoplasmic end of TM1, which were predicted to be in contact with fatty acid chains, were able to collide with this aqueous reagent. Additional evidence for the lipid exposure of MscS came from the results obtained with the DOGS-NTA[Ni(II)]lipids. These results, when combined with information obtained from mobility, O₂, and NiEdda accessibilities, clearly localize the protein within the lipid bilayer. The thickness of a DOPC membrane, ~50 Å,⁴² was used along with the accessibilities obtained with DOGS-NTA[Ni(II)]lipids to determine how MscS sits in the lipid bilayer.

According to the crystal structure, the TM2 helix should be asymmetrically solvated; that is, one surface of this helix should be facing TM1 (buried), while the opposing surface should be solvated by lipids found in crevices between TM1 and TM2 hairpins. However, our model suggests that in the closed state, the TM2 NH₂-terminus faces the lipid bilayer, while its COOH-terminal region is less exposed to the membrane and likely faces TM3, placing TM2 spatially closer to TM3 than what is predicted by the crystal. The TM2 helix is also predicted to be longer, beginning at position T64 instead of F68 (crystal). It remains to be elucidated if the rotation in the membrane plane of the TM3B helix (Fig. 8b) affects the architecture of the cytoplasmic domain and its openings.

While overall exposure to O₂ and NiEdda in TM3 is low when compared to TM1 and TM2, a patch of O₂ accessibilities higher than the TM3 average (positions 104 to 112) was observed (Fig. 2b and c). This hydrophobic area could account for a partially open pore but functionally closed with a region of the permeation path that contains no water, thus blocking ion conduction. Multiple computational studies of water dynamics inside MscS have shown that such scenario is possible^{15,16,18,20} (Supplementary Fig. S8B). Other ion channels trapped in the closed conformation, such as MscL,⁷ the nicotinic acetylcholine receptor,⁴³ KcsA,⁴⁴ and KirBac1.1,⁴⁵ have been shown to maintain a nonconducting pore even if the dimensions of the permeation path are large enough to allow passage of dehydrated ions.

The MscS NH₂-terminal segment model presented here forms a cap at the periplasmic face of the channel. To satisfy our mobility and accessibility data, the final

model displays an NH₂-terminal domain that points away from the permeation pathway and includes 42% of α -helical structure. The function of this segment is unknown, but substitutions at W16 affect the response to negative pressure under patch clamp conditions,⁴⁶ and deletions on the NH₂-terminal segment affect the organization, and perhaps incorporation, of MscS in the lipid bilayer.³⁰ We can then suggest that the NH₂-terminus could also play a potential role in membrane-modulated gating due to its amphipathic nature.

Using a novel refinement method with energy restraints exploiting the information from EPR data, we have rearranged the X-ray structure into a model that represents the closed state. While the final model incorporates as much information as possible from the experiments, there are two limitations of the modeling process that should be noted. First, prediction of a three-dimensional model based only on sequence is difficult, particularly for a multimeric membrane protein. Second, the EPR-derived data presented here represents an average over a large population of channels and, therefore, asymmetry as observed in the crystal structure and MD simulations^{15,17,18,20} cannot be detected. Thus, the presented model is a symmetrized version of MscS. Nevertheless, the power of our approach comes from the pattern of global accessibilities more than the absolute values of a given position, along with the fact that the membrane has well-defined environments that reduce the number of models that can properly fit the experimental constraints. Further structural, spectroscopic, and computational studies will be required to overcome these limitations and to establish the open state of MscS and whether the conformation depicted by the crystal structure is physiologically relevant.

A summary of the proposed closed conformation of the MscS TM domain in a lipid bilayer and a comparison to the crystal conformation is presented in Fig. 8. TM helices are more perpendicular to the plane of the membrane than the helices in the crystal structure. TM1 has two faces, one exposed to the membrane and the other to TM2. TM2 is surrounded by TM1 and TM3, except for its cytoplasmic region that has some exposure to the membrane. In our refined model, the pore is apparently narrower, but how much closer the TM3 helices are to each other cannot be determined in a quantitative manner. The 9° inward motion of TM1–TM2 favoring a more compact structure and the almost horizontal TM3B helix observed during refinement are both in agreement with the motions observed in previous MD studies.¹⁵

Fig. 8. Comparison of MscS crystal structure and outcome of EPR-based refinement. (a) Crystal structure model. Left panel, ribbon representation of the TM segments of MscS (two subunits are shown for clarity). Individual TM segments are color coded as follows: TM1, yellow; TM2, blue; and TM3, red. Rightmost panels show residue environmental parameter profiles mapped onto molecular surfaces of the X-ray model (b) Closed-state model from EPR-based refinement. Left panel, ribbon representation of the MscS closed-state model. Individual TM segments are color coded as above, except for the NH₂-terminus in green. Rightmost panel, residue environmental parameter profiles mapped onto molecular surfaces of the EPR-refined MscS model. The arrows show the key rearrangement in the TM segments of MscS in a native closed state.

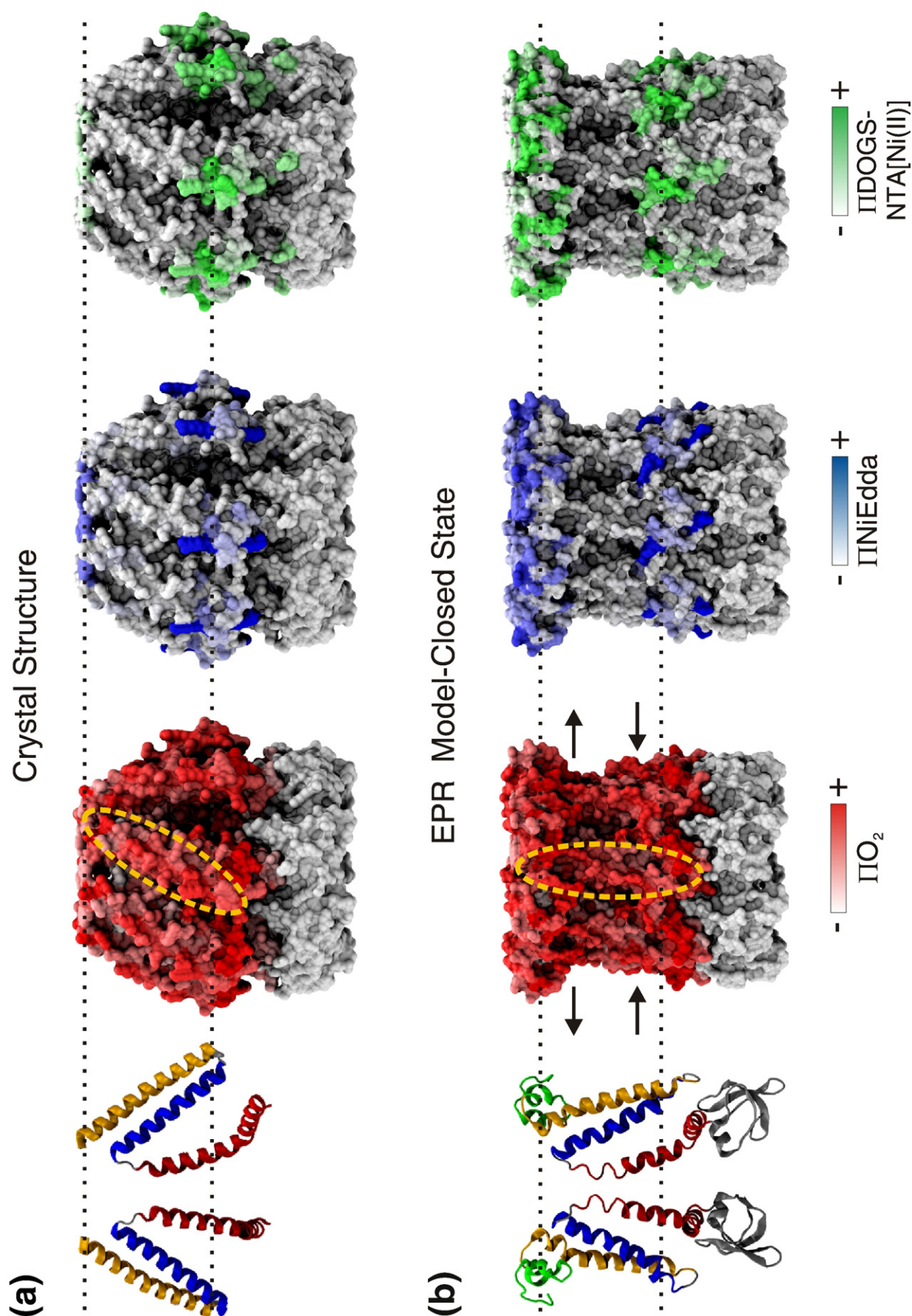


Fig. 8 (legend on previous page)

Finally, the present study also provides some hints on an additional, physiologically relevant function of MscS. Some cysteine mutants produced twice the amount of cells than the WT and other cysteine mutants (after IPTG induction). The respective residues, most of them hydrophobic (W16, V32, V40 and A79), are conserved throughout the MscS family.⁸ Residue W16 has already been shown to participate in the positioning of MscS on the membrane,³⁰ and it does not seem to dramatically affect MscS function (see Fig. 4a and Refs. 30,46). In contrast, when residue V40 was substituted by aspartic acid or lysine, a significant gain of function phenotype (in which cells were not able to grow) was observed, whereas cysteine substitution was tolerated by the cell.⁴⁷ Additionally, cells lacking MS channels exhibit a faster growth rate than other *E. coli* strains (data not shown). Eukaryotic MS channels have been shown to play an important role during mitosis, as the mechanical properties of their membrane change during the cell cycle.^{48–50} Perhaps MscS also plays a role in bacterial cell division.

Experimental Procedures

Mutagenesis, expression, spin labeling, and reconstitution of MscS

Cysteine mutants were generated for residues 2–128 in MscS, covering the NH₂-terminus, TM1, TM2, and TM3. Mutagenesis was performed using the QuickChange™ Site-Directed Mutagenesis Kit (Stratagene). Mutant channels were expressed, purified, labeled, and reconstituted as previously described²⁸ using a pET28 vector containing MscS with a His6 epitope at the NH₂-termini and a pQE70 vector with a His6 epitope at the COOH-termini, for the study of the TM segments and the NH₂-terminus, respectively. MscS-pET28 was used to express the channel in *E. coli* Rosetta™ and MscS-pQE70 was used for expression in *E. coli* M15. The samples were reconstituted at a 750:1 lipid/channel (DOPC:POPG, 6:1) molar ratio by dilution in phosphate-buffered saline in the presence of Bio-beads. To determine the interfacial residues a mixture of DOPC:POPG:DOGS-NTA[Ni(II)]lipids in a 6:2:3 molar ratio was used.

EPR spectroscopy and data analysis

All EPR data were obtained at room temperature. X-band continuous wave EPR spectra were performed as previously described.²² Spectra were obtained in a Bruker EMX spectrometer fitted with a loop gap resonator under the following conditions: 2 mW incident power, 100 kHz modulation frequency, and 1 G modulation. For DOGS-NTA[Ni(II)]lipid experiments, a dielectric resonator was used. The accessibility parameters were quantified as previously reported.^{22,29,51} Briefly, collision frequency is directly proportional to the accessibility of the paramagnetic reagent to the nitroxide, and is defined as

$$\Pi = [\Delta P_{1/2}(X)/P_{1/2}(\text{DPPH})] \times [\Delta H_o(\text{DPPH})/\Delta H_o]$$

where $P_{1/2}(\text{DPPH})$ is the microwave power that saturated the signal relative to that without saturation for a 2,2-

diphenyl-1-picrylhydrazyl crystal (molecule with a single unpaired electron), $\Delta P_{1/2}(X)$ is the difference in $P_{1/2}$ of a given sample exposed to O₂ or NiEdda and N₂. ΔH_o is an estimate of probe mobility derived from the spectral line shape, determined by the degree of averaging of the anisotropic g value.⁵²

Functional assays

Downshock assays were performed as described earlier,⁵³ using the *E. coli* strain MJF465 (kindly donated by Ian Booth).⁴ Method modifications and details were provided earlier.²⁸ In brief, cultures growing in LB and 500 mM NaCl were induced at an OD₆₀₀ of 0.6 with 1 mM IPTG; after being induced for 1 h, the cells were adjusted to an OD₆₀₀ of 1.0, pelleted down, and then resuspended in 50 μ L of fresh LB and 500 mM NaCl. The downshock was made by diluting the cells 1:40 in various shock media ranging from 0 to 500 mM NaCl (pH 7). After 5 min, the cells were serially diluted and 5- μ L aliquots were plated on LB agar. Plated cells were grown overnight, and the colonies were counted and normalized against the OD₆₀₀ (measured right before the downshock).

NH₂-terminal model and pseudoatom-driven solvent accessibility refinement of MscS

An initial, symmetrized model of MscS was built from monomer C of the refined MscS crystal structure (PDB code 2AOU)⁴⁰ including residues 1 to 178. The model included a conformation of the NH₂-terminus obtained using the software Rosetta^{38,39} and applying energy minimization in vacuum (Fig. 6a). In addition to protein atoms, two EPR virtual particles were harmonically attached to each C α atom of the protein, following the method described in Ref. 41 (Sompornpisut *et al.*, unpublished data). The first EPR particle, labeled PROT, was attached on top of the C α atom, while the second EPR particle, representing a spin-label probe, was attached through a bond with a resting length of 6 Å (Fig. 6b).

The water- or lipid-exposed pseudo-spin probes were assigned attractive or repulsive interactions to additional O₂ and NiEdda virtual environment particles, distributed so as to mimic the membrane location, while the buried pseudo-spins were allowed to artificially overlap with the backbone core (PROT particles). Assignment of interactions was performed based on EPR accessibilities as indicated in the text.

Structural refinement simulations were performed using the CHARMM program version c32a2⁵⁴ modified to implement the novel methodology. The extended atom PARAM19 force field was modified to reduce the effect of charged residues in vacuum according to the scheme in Ref. 55. Harmonic restraints were applied to keep O₂ particles away from the MscS pore, to keep residues 5, 23, 53, 57, 60, and 127 at the membrane–water interface, and to force side chains of residues 23 and 27 to face away from the center of the channel. In addition, RMSD constraints were applied (to maintain the initial secondary structure) to residues 10–14, 20–26, 29–57, 68–91, 96–113, 114–128, and 129–178. Multiple minimization and equilibration cycles were performed. After 10 million steps (1 fs per time step), the NH₂-terminus was rotated and further equilibration was carried out. Closed-state model from EPR-based refinement†.

† <http://www.ks.uiuc.edu/~sotomayo/MSCSEPR/>

Acknowledgements

The authors thank J. Cordero-Morales, P. Sompornpisut, S. Chakrapani, C. Ptak, L. Cuello, V. Jogini, and H. Raghuraman for providing comments and experimental advice. This work was supported by the National Institutes of Health grants GM063617 (E.P.), P41-RR05969 (K.S.), 1 R01 GM067887 (K.S.), and GM-62342 (B.R.). M.S and K.S. also acknowledge supercomputer time provided through NSF grant LRAC MCA93S028. Data mapping and molecular images were done using VMD,⁵⁶ its data-import plugin, and Tachyon.⁵⁷ The authors declare that they have no competing financial interests.

Supplementary Data

Supplementary data associated with this article can be found, in the online version, at [doi:10.1016/j.jmb.2007.10.086](https://doi.org/10.1016/j.jmb.2007.10.086)

References

- Wood, J. M. (1999). Osmosensing by bacteria: signals and membrane-based sensors. *Microbiol. Mol. Biol. Rev.* **63**, 230–262.
- Hamill, O. P. & Martinac, B. (2001). Molecular basis of mechanotransduction in living cells. *Physiol. Rev.* **81**, 685–740.
- Poolman, B., Blount, P., Folgering, J. H., Friesen, R. H., Moe, P. C. & van der Heide, T. (2002). How do membrane proteins sense water stress? *Mol. Microbiol.* **44**, 889–902.
- Levina, N., Totemeyer, S., Stokes, N. R., Louis, P., Jones, M. A. & Booth, I. R. (1999). Protection of *Escherichia coli* cells against extreme turgor by activation of MscS and MscL mechanosensitive channels: identification of genes required for MscS activity. *EMBO J.* **18**, 1730–1737.
- Martinac, B., Buechner, M., Delcour, A. H., Adler, J. & Kung, C. (1987). Pressure-sensitive ion channel in *Escherichia coli*. *Proc. Natl Acad. Sci. USA*, **84**, 2297–2301.
- Berrier, C., Besnard, M., Ajouz, B., Coulombe, A. & Ghazi, A. (1996). Multiple mechanosensitive ion channels from *Escherichia coli*, activated at different thresholds of applied pressure. *J. Membr. Biol.* **151**, 175–187.
- Chang, G., Spencer, R. H., Lee, A. T., Barclay, M. T. & Rees, D. C. (1998). Structure of the MscL homolog from *Mycobacterium tuberculosis*: a gated mechanosensitive ion channel. *Science*, **282**, 2220–2226.
- Bass, R. B., Strop, P., Barclay, M. & Rees, D. C. (2002). Crystal structure of *Escherichia coli* MscS, a voltage-modulated and mechanosensitive channel. *Science*, **298**, 1582–1587.
- Perozo, E., Kloda, A., Cortes, D. M. & Martinac, B. (2001). Site-directed spin-labeling analysis of reconstituted MscL in the closed state. *J. Gen. Physiol.* **118**, 193–206.
- Sukharev, S., Betanzos, M., Chiang, C. S. & Guy, H. R. (2001). The gating mechanism of the large mechanosensitive channel MscL. *Nature*, **409**, 720–724.
- Perozo, E., Cortes, D. M., Sompornpisut, P., Kloda, A. & Martinac, B. (2002). Open channel structure of MscL and the gating mechanism of mechanosensitive channels. *Nature*, **418**, 942–948.
- Perozo, E., Kloda, A., Cortes, D. M. & Martinac, B. (2002). Physical principles underlying the transduction of bilayer deformation forces during mechanosensitive channel gating. *Nat. Struct. Biol.* **9**, 696–703.
- Anishkin, A., Gendel, V., Sharifi, N. A., Chiang, C. S., Shirinian, L., Guy, H. R. & Sukharev, S. (2003). On the conformation of the COOH-terminal domain of the large mechanosensitive channel MscL. *J. Gen. Physiol.* **121**, 227–244.
- Gullingsrud, J. & Schulten, K. (2003). Gating of MscL studied by steered molecular dynamics. *Biophys. J.* **85**, 2087–2099.
- Sotomayor, M. & Schulten, K. (2004). Molecular dynamics study of gating in the mechanosensitive channel of small conductance MscS. *Biophys. J.* **87**, 3050–3065.
- Anishkin, A. & Sukharev, S. (2004). Water dynamics and dewetting transitions in the small mechanosensitive channel MscS. *Biophys. J.* **86**, 2883–2895.
- Sotomayor, M., van der Straaten, T. A., Ravaioli, U. & Schulten, K. (2006). Electrostatic properties of the mechanosensitive channel of small conductance MscS. *Biophys. J.* **90**, 3496–3510.
- Sprink, S. A., Elmore, D. E. & Dougherty, D. A. (2006). Voltage-dependent hydration and conduction properties of the hydrophobic pore of the mechanosensitive channel of small conductance. *Biophys. J.* **90**, 3555–3569.
- Vora, T., Corry, B. & Chung, S. H. (2006). Brownian dynamics investigation into the conductance state of the MscS channel crystal structure. *Biochim. Biophys. Acta*, **1758**, 730–737.
- Sotomayor, M., Vasquez, V., Perozo, E. & Schulten, K. (2007). Ion conduction through MscS as determined by electrophysiology and simulation. *Biophys. J.* **92**, 886–902.
- McHaourab, H. S., Lietzow, M. A., Hideg, K. & Hubbell, W. L. (1996). Motion of spin-labeled side chains in T4 lysozyme. Correlation with protein structure and dynamics. *Biochemistry*, **35**, 7692–7704.
- Perozo, E., Cortes, D. M. & Cuello, L. G. (1998). Three-dimensional architecture and gating mechanism of a K⁺ channel studied by EPR spectroscopy. *Nat. Struct. Biol.* **5**, 459–469.
- Cuello, L. G., Cortes, D. M. & Perozo, E. (2004). Molecular architecture of the KvAP voltage-dependent K⁺ channel in a lipid bilayer. *Science*, **306**, 491–495.
- Columbus, L., Kalai, T., Jeko, J., Hideg, K. & Hubbell, W. L. (2001). Molecular motion of spin labeled side chains in alpha-helices: analysis by variation of side chain structure. *Biochemistry*, **40**, 3828–3846.
- Koteiche, H. A. & McHaourab, H. S. (1999). Folding pattern of the alpha-crystallin domain in alphaA-crystallin determined by site-directed spin labeling. *J. Mol. Biol.* **294**, 561–577.
- Perozo, E., Cortes, D. M. & Cuello, L. G. (1999). Structural rearrangements underlying K⁺-channel activation gating. *Science*, **285**, 73–78.
- Cortes, D. M., Cuello, L. G. & Perozo, E. (2001). Molecular architecture of full-length KcsA: role of cytoplasmic domains in ion permeation and activation gating. *J. Gen. Physiol.* **117**, 165–180.
- Vasquez, V., Cortes, D. M., Furukawa, H. & Perozo, E. (2007). An optimized purification and reconstitution method for the MscS channel: strategies for spectroscopic analysis. *Biochemistry*, **46**, 6766–6773.
- Gross, A. & Hubbell, W. L. (2002). Identification of protein side chains near the membrane-aqueous

- interface: a site-directed spin labeling study of KcsA. *Biochemistry*, **41**, 1123–1128.
30. Miller, S., Bartlett, W., Chandrasekaran, S., Simpson, S., Edwards, M. & Booth, I. R. (2003). Domain organization of the MscS mechanosensitive channel of *Escherichia coli*. *EMBO J.* **22**, 36–46.
 31. Miller, S., Edwards, M. D., Ozdemir, C. & Booth, I. R. (2003). The closed structure of the MscS mechanosensitive channel. Cross-linking of single cysteine mutants. *J. Biol. Chem.* **278**, 32246–32250.
 32. Edwards, M. D., Li, Y., Kim, S., Miller, S., Bartlett, W., Black, S. *et al.* (2005). Pivotal role of the glycine-rich TM3 helix in gating the MscS mechanosensitive channel. *Nat. Struct. Mol. Biol.* **12**, 113–119.
 33. Takeshi, N., Sokabe, M. & Yoshimura, K. (2006). Lipid–protein interaction of the MscS mechanosensitive channel examined by scanning mutagenesis. *Biophys. J.*
 34. Koprowski, P. & Kubalski, A. (2003). C termini of the *Escherichia coli* mechanosensitive ion channel (MscS) move apart upon the channel opening. *J. Biol. Chem.* **278**, 11237–11245.
 35. Schumann, U., Edwards, M. D., Li, C. & Booth, I. R. (2004). The conserved carboxy-terminus of the MscS mechanosensitive channel is not essential but increases stability and activity. *FEBS Lett.* **572**, 233–237.
 36. Cornette, J. L., Cease, K. B., Margalit, H., Spouge, J. L., Berzofsky, J. A. & DeLisi, C. (1987). Hydrophobicity scales and computational techniques for detecting amphipathic structures in proteins. *J. Mol. Biol.* **195**, 659–685.
 37. Rees, D. C., DeAntonio, L. & Eisenberg, D. (1989). Hydrophobic organization of membrane proteins. *Science*, **245**, 510–513.
 38. Simons, K. T., Kooperberg, C., Huang, E. & Baker, D. (1997). Assembly of protein tertiary structures from fragments with similar local sequences using simulated annealing and Bayesian scoring functions. *J. Mol. Biol.* **268**, 209–225.
 39. Bonneau, R., Strauss, C. E., Rohl, C. A., Chivian, D., Bradley, P., Malmstrom, L. *et al.* (2002). De novo prediction of three-dimensional structures for major protein families. *J. Mol. Biol.* **322**, 65–78.
 40. Steinbacher, S., Bass, R., Strop, P. & Rees, D. C. (2007). Structures of the prokaryotic mechanosensitive channels MscL and MscS. In *Current Topics in Membranes. Mechanosensitive Ion Channels, Part A* (Hamill, O. P., ed), vol. 58, pp. 1–24, Elsevier Inc., New York, NY.
 41. Jiang, Y., Lee, A., Chen, J., Ruta, V., Cadene, M., Chait, B. T. & MacKinnon, R. (2003). X-ray structure of a voltage-dependent K⁺ channel. *Nature*, **423**, 33–41.
 42. Wiener, M. C. & White, S. H. (1992). Structure of a fluid dioleoylphosphatidylcholine bilayer determined by joint refinement of x-ray and neutron diffraction data. III. Complete structure. *Biophys. J.* **61**, 434–447.
 43. Miyazawa, A., Fujiyoshi, Y. & Unwin, N. (2003). Structure and gating mechanism of the acetylcholine receptor pore. *Nature*, **423**, 949–955.
 44. Doyle, D. A., Morais Cabral, J., Pfuetzner, R. A., Kuo, A., Gulbis, J. M., Cohen, S. L. *et al.* (1998). The structure of the potassium channel: molecular basis of K⁺ conduction and selectivity. *Science*, **280**, 69–77.
 45. Kuo, A., Gulbis, J. M., Antcliff, J. F., Rahman, T., Lowe, E. D., Zimmer, J. *et al.* (2003). Crystal structure of the potassium channel KirBac1.1 in the closed state. *Science*, **300**, 1922–1926.
 46. Rasmussen, A., Rasmussen, T., Edwards, M. D., Schauer, D., Schumann, U., Miller, S. & Booth, I. R. (2007). The role of tryptophan residues in the function and stability of the mechanosensitive channel MscS from *Escherichia coli*. *Biochemistry*, **46**, 10899–10908.
 47. Okada, K., Moe, P. C. & Blount, P. (2002). Functional design of bacterial mechanosensitive channels. Comparisons and contrasts illuminated by random mutagenesis. *J. Biol. Chem.* **277**, 27682–27688.
 48. Zhou, X. L. & Kung, C. (1992). A mechanosensitive ion channel in *Schizosaccharomyces pombe*. *EMBO J.* **11**, 2869–2875.
 49. Rundle, D. R., Gorbisky, G. & Tsiokas, L. (2004). PKD2 interacts and co-localizes with mDia1 to mitotic spindles of dividing cells: role of mDia1 IN PKD2 localization to mitotic spindles. *J. Biol. Chem.* **279**, 29728–29739.
 50. Haswell, E. S. & Meyerowitz, E. M. (2006). MscS-like proteins control plastid size and shape in *Arabidopsis thaliana*. *Curr. Biol.* **16**, 1–11.
 51. Farahbakhsh, Z. T., Altenbach, C. & Hubbell, W. L. (1992). Spin labeled cysteines as sensors for protein–lipid interaction and conformation in rhodopsin. *Photochem. Photobiol.* **56**, 1019–1033.
 52. McHaourab, H. S. & Perozo, E. (2002). Determination of protein folds and conformational dynamics using spin-labeling EPR spectroscopy. In *Biological Magnetic Resonance* (Berliner, L. J., Eaton, S. S. & Eaton, G. R., eds), vol. 19, pp. 185–248, Springer, New York, NY.
 53. Batiza, A. F., Kuo, M. M., Yoshimura, K. & Kung, C. (2002). Gating the bacterial mechanosensitive channel MscL in vivo. *Proc. Natl. Acad. Sci. USA*, **99**, 5643–5648.
 54. Brooks, B., Bruccoleri, R. E., Olafson, B. D., States, D. J., Swaminathan, S. & Karplus, M. (1983). CHARMM: a program for macromolecular energy, minimization, and dynamics calculations. *J. Comput. Chem.* **4**, 187–217.
 55. Lazaridis, T. & Karplus, M. (1999). Effective energy function for proteins in solution. *Proteins*, **35**, 133–152.
 56. Humphrey, W., Dalke, A. & Schulten, K. (1996). VMD: visual molecular dynamics. *J. Mol. Graphics*, **14**, 33–38, 27–28.
 57. Stone, J. (1998). *An Efficient Library for Parallel Ray Tracing and Animation*. Master's thesis, University of Missouri-Rolla, Rolla, MO.